A SINGLE MOLECULE STUDY ON THE STRUCTURAL BASIS OF ION SELECTIVE PERMEATION IN VOLTAGE-GATED SODIUM CHANNELS

A THESIS IN

Cellular and Molecular Biology

Presented to the Faculty of the University
of Missouri-Kansas City in partial fulfillment of
the requirements for the degree

MASTER OF SCIENCE

By
JOSHUA VANCE

B.S. University of Missouri-Columbia, 2017

Kansas City, Missouri

2021

A SINGLE MOLECULE STUDY ON THE STRUCTURAL BASIS OF ION SELECTIVE PERMEATION IN VOLTAGE-GATED SODIUM CHANNELS

Joshua Vance, Candidate for the Master of Science Degree

University of Missouri-Kansas City, 2021

ABSTRACT

High resolution studies of voltage-gated sodium channels (VGSCs) can not reveal the dynamic nature of the channel structures, especially in lipid environments, which are vital for rational drug design. The bacterial NavAb channel is highly like its eukaryotic orthologs in structure, function, and pharmacological profiles, serving as an ideal model for biochemical characterizations. I purified the NavAb channel proteins and reconstituted them into liposomes. With liposome flux assays, I showed that the purified NavAb channels are highly conductive for Na^+ and H^+, but less permeable to K^+, Cs^+, and the bulky cation N-methyl-D-Glucamine. The NavAb channel is cysteine free, which allowed for introduction of cysteine mutations at different sites to be labeled with fluorophores. Thus, the structural dynamics of the NavAb channel can be examined utilizing single-molecule FRET. It is proposed that the ion selectivity of VGSCs is based on the size and charge, implying very minimized flexibilities in the selectivity filter. However, it was found that selectivity collapse underlies the slow inactivation in VGSC, including NavAb. To address the discrepancies, I examined the structural dynamics of the NavAb selectivity

filter under different ionic conditions and membrane voltages. Surprisingly, my smFRET data showed large spontaneous FRET transitions which suggest significant structural dynamics at the NavAb selectivity filter. Moreover, I also detected significant FRET changes at the NavAb selectivity filter induced by activating voltage. My results indicate that ion selectivity in VGSC is not completely based on size and charge and needs to be investigated further.

APPROVAL PAGE

The faculty listed below, appointed by the Dean of the School of Biological and Chemical Science, have examined a thesis titled "A single molecule study on the structural basis of ion selective permeation in voltage-gated sodium and calcium channels" presented by Joshua Vance, candidate for the Master of Science degree and certify that in their opinion it is worthy of acceptance.

Supervisory Committee

Shizhen "Jeff" Wang, Ph.D.
Department of Cell and Molecular Biology and Biochemistry

Xiaolan Yao, Ph.D.
Department of Cell and Molecular Biology and Biochemistry

Xiangping Chu, M.D, Ph.D.
School of Medicine

CONTENTS

LIST OF ILLUSTRATIONS

Figure Page

LIST OF TABLES

Table page

ACKNOWLEDGEMENTS

I would like to thank Dr. Shizhen Wang for all his help and guidance throughout this process. I would like to thank Dr. Shuo Han for teaching me a multitude of useful techniques for the lab. I would like to thank my parents and grandparents for their prayers and well wishes. I would like to thank my girlfriend Cassie Ballew for encouraging me throughout this process despite timetables being shifted a few times

CHAPTER 1

INTRODUCTION

1.1 Voltage-gated Ion Channels

Voltage-gated sodium and calcium channels propagate electrical signals in electrically excitable cells such as nerve and muscle cells (Payandeh 2011; Hille 1975). They are associated with numerous human diseases including cardiac arrhythmia, chronic pain, and epilepsy (Catterall 2015), and serve as the molecular target of a plethora of drugs currently in clinical use such as the local anesthetic lidocaine, antiarrhythmic flecainide, and antihypertensive amlodipine. Advancement of mechanistic understandings on the function and regulation of sodium and calcium channels will improve our ability to develop therapies with higher efficacies and specificities.

Electrophysiological studies by Hodgkin and Huxley on the giant squid axon showed that the electrical signals, known as action potentials, were caused by the selective movement of ions across the membrane barrier. These ionic movements are mediated by voltage-gated ion channels. (Hodgkin 1952). Their work showed that an action potential is triggered by sodium influx into the cell following the electrochemical gradient, depolarizing the membrane potential. Within milliseconds sodium inflow is diminished by the inactivation of voltage-gated sodium channels, meanwhile, the voltage-gated potassium is opened to conduct potassium into cells to repolarize the membrane potential. This groundbreaking discovery led to future work by Hille, whose research explained the ion selectivity of the voltage-gated sodium channels with a four-barrier three-site model of the sodium selectivity filter. With the model, he elegantly showed how sodium channel blocking drugs such as local anesthetic

lidocaine act by binding to receptor sites within the voltage-gated sodium channel pore (Hille 1975).

A leap forward in determining the structure of the voltage-gated sodium channel protein was achieved by the Catterall et al group, who isolated the voltage-gated sodium channel using scorpion toxin as a chemical bait. They revealed the molecular compositions of the eukaryotic voltage-gated sodium channel and showed that it is composed of a large pore-forming alpha subunit and two smaller beta subunits modifying channel gating dynamics (Beneski 1980). The large pore-forming alpha subunit is composed of 24 transmembrane segments, each with four homologous domains with six transmembrane segments (Beneski 1980).

1.2 Prokaryotic and Eukaryotic VGSCs

The pore-forming units of the eukaryotic Nav channels are very large and contain multiple post-translational modification sites. In recent years, due to the breakthrough in the single particle reconstruction cryo-EM technique, many high-resolution structures of the eukaryotic sodium voltage channels (Navs) and calcium voltage channels (Cavs), in complex with auxiliary subunits were obtained. However, it is still very challenging to obtain sufficient pure, stable and homogenous eukaryotic Nav and Cav channel proteins for biochemical characterizations of their structure and function. This challenge has encouraged the identification of the prokaryotic orthologs such as the NaChBac family (Yue 2002), which provided cost-effective model Nav channels to circumvent these technical barriers. NavAb is a member of the NaChBac family and became the first VGSC with its crystal structure solved. Unlike the eukaryotic Nav channels, NavAb channel functions as homotetramers (Catterall 2020), and its pore-forming subunit is much smaller than eukaryotic Navs. As a result, it is a

much easier VGSC to work with than its bulky eukaryotic orthologs that are characterized by large size, multiple post translational modifications, which can only be expressed in mammalian cells (Catterall 2020).

Since cryo-EM studies have revealed the atomic structures of many eukaryotic voltage-gated sodium and calcium channels, they all exhibit remarkable similarities with the prokaryotic NavAb (Tang 2014; Payandeh 2011). In terms of the pharmacological profiles, the prokaryotic NavAb channel is also very similar to its eukaryotic orthologs and can be regulated by many blockers of the eukaryotic Nav and Cav channels with similar affinities (Tang 2016; Catterall 2020). This data suggests that NavAb is a valid model voltage-gated sodium channel for studying the mechanisms of voltage sensing and gating, as well as the pharmacology of the eukaryotic Navs and Cavs. Crystal structures of the NavAb channel have offered invaluable insights into the atomic architecture of the NavAb channel. The ion permeation pore of the NavAb consists of the S5 and S6 transmembrane segments with a selectivity filter at the extracellular side and a voltage sensor. The voltage sensor is composed of 4 transmembrane segments, named S1 through S4. The voltage sensor of NavAb is coupled to the pore-forming domain through a short helical S4-5 linker, which is the key structural element that transduces conformational changes from the voltage sensor to the pore-forming domain (Wisedchaisri 2019). Like eukaryotic Navs, electrophysiological studies showed that the NavAb channel opens upon depolarizing voltage with similar ion selectivity profiles as that of eukaryotic Navs. The key difference is that the NavAb channel lacks the fast inactivation gate of eukaryotic Navs. However, NavAb does enter a low conductive state shortly after activation, called slow inactivation, which is also observed in many eukaryotic Navs. Mutational studies have

identified the selectivity filter of the NavAb channel may enter a collapse conformation during slow inactivation, which also occurs in eukaryotic Nav and Cav channels (Catterall 2020).

1.3 Structural Basis of Ion Selectivity in NavAb

The ion selectivity of Navs originates primarily in the selectivity filter region, a helix-loop-helix motif between transmembrane segments S5-S6 forming ion permeation pore (Catterall 2020). The selectivity filter pore of the NavAb channel is lined by the residues S178, E177 (HFS, high field strength site), L176, and T175 (Chakrabarti 2013) from the 4 identical subunits. The lining residues of the eukaryotic selectivity pore are from four homologous, but not identical domains, forming a distinctive HFS which plays a key role in determining their ion selectivity. In the NavAb channel, the outward-facing edge of the HFS region of the selectivity filter is composed of four Glu residues (EEEE) from the 4 identical subunits. However, the eukaryotic HFS in Navs have the Asp-Glu-Lys-Ala (DEKA) signature sequence and the eukaryotic Cavs have the signature sequence of EEEE (Heinemann 1992). Mutations in the DEKA region greatly reduce sodium selectivity in eukaryotic Navs (Heinemann 1992). The difference in HFS site residues between the prokaryotic and eukaryotic voltage-gated sodium channels presents a mechanistic question: how does the NavAb channel achieve its sodium selectivity with its highly negative HFS site commonly seen in eukaryotic Cav channels? One hypothesis is that in NavAb the Glu residues lining the HFS site undergo rapid dunking in the presence of ions (Chakrabarti 2013), which was not seen in eukaryotic HFS. Such dunking motions may not be necessary for eukaryotic channels because the positively charged Lys and hydrophobic Ala residues could perhaps compensate for the asymmetry of the partially hydrated sodium ions (Hille 1975; Catterall 2020; Chakrabarti 2013). In sharp contrast, K channels conduct only full dehydrated ions, which may require more symmetrical

binding sites within the selectivity filter pore (Payandeh 2011). Sodium conduction by NavAb is potentially achieved with trigonal bipyramidal coordination with 1-2 water molecules interacting with Na ions in the selectivity pore. Therefore, structurally it only requires one of the 4 Glu residues to interact with the Na ions, thus the conductive conformations of the NavAb selectivity filter pore could be highly asymmetric. This lack of symmetry is in contrast with K selective channels where the selectivity filter is highly symmetrical in the presence of K ions (Wang 2016). The HFS sites of Navs and Cavs contain multiple negatively charged residues with oxygen groups that potentially interact with permeating ions. In contrast to the eukaryotic HFS, the prokaryotic channel NavAb uses EEEE within its HFS, while the introduction of triple Asp mutations in the HFS can convert the sodium selective NavAb into a calcium selective channel, called the CavAb channel (Payandeh 2011; Tang 2014). It remains unclear why eukaryotic Navs have a selectivity filter with slightly different residues at HFS, yet still be able to selectively conduct sodium ions, where the structural dynamics may play a determinant role.

1.4. Pharmacology of Voltage-Gated Sodium Channels

As previously described, voltage-gated sodium channels are molecular targets of many first-line drug molecules. For example, drugs for the treatment of epilepsy (phenytoin, carbamazepine, lidocaine), chronic pain (lidocaine), and cardiac arrhythmia (Quinidine, lidocaine) are all blockers of VGSC. These drugs act on the human Navs in a state-dependent manner, either in a voltage-dependent or frequency-dependent manner (Hondeghem 1984; Catterall 2020). The voltage-dependent blockers exhibit stronger inhibitory effects in depolarized damaged channels that trigger excess action potentials (Catterall 2020). Frequency-dependent block leads to more potent inhibition in rapidly firing channels, for

example, the VGSCs that transmit pain signals constantly (Catterall 2020). Both voltage and frequency-dependent blocking are important mechanisms underlying the therapeutic efficacies of VGSC blocking drugs. By targeting hyperactive channels, the VGSC blocking drugs (such as lidocaine) can provide relief without significant side effects resulting from non-specific blocking of other homologous voltage-gated ion channels.

The drug receptor sites of voltage-gated sodium channels were originally mapped by site-directed mutagenesis analyses, which have identified many key amino acid residues involved in drug regulation. Mapping of these residues to the eukaryotic Nav channel structures showed that the S6 segments from domain I, II and IV form the drug receptor sites for lidocaine and flecainide (Nau 2003, Catterall 2020). These results are further supported by the NavAb crystal structures in complex with lidocaine and flecainide (El-Din 2018). The electron density maps clearly showed the bound lidocaine in the central cavity, which is immediately underneath the selectivity filter at the intracellular outlet (Catterall 2020). Binding at the intracellular outlet may cause a complete block of ion flow, including protons. Flecainide binds at a similar site but occupies a larger space in the central cavity (El-Din 2018). Both flecainide and lidocaine have their essential protonated amino groups projected into the ion selectivity filter pore, where they potentially interact with backbone carbonyl oxygens of the Thr175. The structures provide a rationale for their potential impacts on the structural dynamics of the Nav selectivity filter. Structural basis for fenestration presences within NavAb channel was established using crystallographic studies on open pore Nav channels, which revealed a small hole about 10.5 angstroms in diameter (Lienaeus 2017). This is a sufficient size for lidocaine entry from the lipid phase, most likely during the open activation state. Blocking the fenestration pore by mutations greatly decreased drug effectiveness especially on

larger drug molecules (El-Din 2018). The fenestration pore allows the drug molecule to directly enter the central cavity from the lipid phase, as shown by crystallographic studies. More importantly, these fenestrations are also found in eukaryotic Nav channels and play important roles in determining the efficacies of these drug molecules.

1.5 Functional Characterization of NavAb Proteins

So far, all the functional studies on the NavAb channel were performed on these recombinantly expressed insect cells. Therefore, it remains unclear whether the NavAb channel proteins expressed and purified in *E. coli* cells still retain their native function as a voltage-gated sodium channel. To address the question, we expressed and purified the NavAb proteins and reconstituted them into liposomes containing POPE/POPG (3/1). With high KCl inside and K ionophore valinomycin, the Nernst electrical potential was generated to drive proton or sodium uptake through the NavAb channel proteins, if they are functional. The proton uptake through the NavAb channel then protonates and quenches the fluorophore probe ACMA. Thus, the channel function of the NavAb channel can be determined by measuring the quenching of ACMA fluorescent emissions in a high throughput manner. These studies will validate whether purified NavAb proteins are a valid model Nav channel for further biochemical and biophysical characterizations.

1.6 Studying Structural Dynamics of NavAb Channel using smFRET

The selectivity filter of the NavAb channel determines its ion selectivity. Electrophysiological studies showed that the NavAb selectivity filter has three distinct conformations, open, closed, and inactivated (Payandeh 2011). However, proteins for high resolution studies were deeply frozen so that the conformation dynamics of the NavAb proteins were dramatically minimized. More importantly, both crystallography and cryo-EM methods,

in principle, are biased against conformations that are highly dynamic, less abundant, or symmetric. Therefore, the mechanistic insights from these high-resolution structures remained to be validated, especially voltage-gated ion channels, due to the inability to control the channel gating status by applying non-zero voltages on channel proteins in solution environments. In this regard, single molecule fluorescence resonance energy transfer (smFRET) can report the unsynchronized real time conformational trajectories of the voltage-gated ion channels in lipid environment at different voltages, combining with single channel recordings, can provide mechanistic insights into voltage sensing and gating that are unattainable previously (Roy 2008). Previous single-molecule FRET studies on the KirBac channel uncovered the structural dynamics of the potassium selectivity filter and channel gates, led to novel models to explain the ligand gating of the Kir channels and the structural basis of ion selectivity (Wang 2016).

As described previously, the voltage-gated sodium channel conducts partially dehydrated sodium ions, and it was proposed that the channel's ion selectivity originates from selection by size and charge. However, the central presumption of the above model depends on the structural dynamics and flexibility of the selectivity filter, which remain to be experimentally determined. By constructing tandem NavAb channels, we were able to introduce two cysteine residues within the tetrameric NavAb channel unit, one pair at a time, at different sites of the NavAb selectivity filter. We labeled the mutant proteins with the FRET fluorophore pair Alexa Fluor 555 and 647 c2 maleimide and then implemented smFRET studies on the labeled NavAb channels reconstituted into liposomes to evaluate the structural dynamics of the selectivity filter. Molecular simulations from crystal structures have suggested that ion concentration and type play a role in how ions are conducted through the selectivity filter and that sodium ions are more likely to occupy the ion pass-by site (Callahan 2018). This

site occupation could potentially alter selectivity filter dynamics, which could be detected by smFRET measurements under different ionic conditions. These studies will provide new insights into potential interactions between the selectivity filter and cations that are highly permeable as well as those low or not permeable. Lidocaine blocks NavAb by binding to the central cavity immediately underneath the selectivity filter and physically blocking ion conductance (El-Din 2018). It has been shown that lidocaine may destabilize the resting state by causing large hyperpolarizing shifts in the voltage sensor domain (Arcisio-Miranda 2010). However, it is still unknown whether lidocaine will affect the conformation of the selectivity filter as well. In summary, studying the structural dynamics of the NavAb selectivity filter by smFRET will reveal its real time conformational changes and dynamics under different ionic conditions, voltages, and drugs, therefore providing fundamental mechanistic insights into ion selectivity, slow inactivation, and drug modulation.

CHAPTER 2

MATERIALS AND METHODS

2.1 Plasmids

All the plasmids used in the present work were listed in Table 1. The cDNA of the NavAb channel with N49K mutation was codon optimized and subcloned into pET28a vector by NdeI and BamHI sites (kindly provided by Dr. Katsumasa Irie of Nagoya University, Japan). The resulting NavAb protein carries a N-terminal 6x Histag following by a thrombin protease (LVPRGS) cutting site. For tandem dimer and tetramer constructs, the NavAb monomers were linked by a flexible linker containing 1 thrombin cutting site and 'GGGSGGGS' residues. All the cysteine mutations were introduced by site-direct mutagenesis then confirmed by DNA sequencing.

Table 2.1 The NavAb channel plasmids and their resulting topology

Name	Vector	Restriction sites	Channel promoter topology	Protomers/ channel
NavAb1m-WT	pET-28a	NdeI-BamHI	6*His-NavAb[WT]	Tetramer
NavAb2m-E189C-WT	pET-28a	NdeI-SalI	6*His-NavAb[E189C]-NavAb[WT]	Dimer
NavAb2m-E189C-WT	pET-28a	NdeI-SalI	6*His-NavAb[V190C]-NavAb[WT]	Dimer
NavAb4m-E189C2-WT2	pET-28a	NdeI-XhoI	6*His-NavAb[E189C]-NavAb[E189C]-NavAb[WT]-NavAb[WT]	Monomer
NavAb4m-V190C2-WT2	pET-28a	NdeI-XhoI	6*His-NavAb[V190C]-NavAb[V190C]-NavAb[WT]-NavAb[WT]	Monomer

2.2 Expression of the NavAb Channels

Escherichia coli KRX competent cells were used for the expression of all NavAb channel proteins. The competent cells were allowed to thaw on ice (4 °C) for 5 min, then 1 uL NavAb plasmids were added and incubated on ice for 30 min. After incubation, 0.5 ml SOC medium (or LB) was added and the transformants were incubated at 225 rpm for 1 hour at 37 °C, then pelleted and spread on plates containing 50 ug/ml of Kanamycin. To express NavAb channels, the transformant cells were inoculated into LB medium containing 50ug/ml Kanamycin then incubated in the shaker at 225rpm at 37C until OD_{600} reached 0.5-0.6. Then the temperature was decreased to 22 °C for 1 hour and 0.1 mM Isopropyl B-D-1-thiogalactopyranoside (IPTG) and 0.1% L-rhamnose (w/v) were added to induce expression overnight (16-18 hours). The cells were harvested and resuspended into a buffer containing 20 mM Tris-HCl, 150 mM NaCl, 20 mM imidazole, pH 8, at a ratio of 20ml of buffer per liter of culture.

2.3 Purification of the NavAb Channel Proteins

The cell resuspensions expressing NavAb channels were added with proteinase inhibitor cocktail (2 mM PMSF, 1 mM AEBSF, 1.5 uM Pepstatin, 1.4 uM E-64, 4 uM Bestatin), 1 mM TCEP (for cysteine mutants only), 1mg/ml DNaseI. The cells were broken by a microfluidizer at 30,000 PSI pressure, then centrifuged at 16,000x g, at 4 °C to remove unbroken cells, debris, and inclusion bodies. The supernatants were further centrifuged at 32,000 rpm for 3 hours at 4 °C to collect membrane fractions. The membranes were resuspended in a buffer containing 20 mM Tris-HCl, 150 mM NaCl, 20 mM imidazole, pH 8.0, then either frozen in -80 °C freezer or subjected for purification immediately. To extract the NavAb protein, LMNG detergent was added at a final concentration of 1% (w/v) then

incubated at 4 °C for 3 hours. The solubilized membranes were then centrifuged at 16,000x g to remove insoluble then mixed with 0.2 ml cobalt beads for 1 hour at 4 °C. The cobalt beads were washed with >30x bed volumes of washing buffer containing 20mM Tris, 150 mM NaCl, 0.1% LMNG, 20 mM imidazole, pH 8.0, then the NavAb channel proteins were eluted with elution buffer containing 20mM Tris, 150 mM NaCl, 0.1% LMNG, 450 mM Imidazole, pH 8.0. For cysteine mutants, 1 mM TCEP was always included in the resuspension, washing and elution buffers.

2.4 Fluorophore Labeling of the NavAb Cysteine Mutant Proteins

The affinity purified NavAb proteins were passed through a desalting column to change the buffer into 20 mM Tris-HCL, 150 mM NaCl, 0.1% LMNG pH 7.0 for fluorophore labeling, which is essential for protonation of primary amine groups in the NavAb proteins to reduce size reactions between the amine and maleimide groups. After buffer exchange, the NavAb proteins were mixed with FRET fluorophores (Alexa Fluor 555 and 647 c2 maleimide, 1:1) with a protein dye ratio of 1:5 and then incubated for 1 hour in a dark container to avoid photobleaching of the fluorophores. The labeling reaction was then stopped by adding 2mM β-mercaptoethanol and additional 30 min incubation. The fluorophore labeled NavAb proteins were then subjected to another round of affinity purification using cobalt resin, to remove the free fluorophores completely. Proteins were then loaded onto Superdex 200 size exclusion column with a running buffer containing 20 mM Tris-HCl, 150 mM NaCl, 0.1% LMNG, 1 mM TCEP, pH 7.0. The tetramer fraction with peak at about 11 ml were collected and concentrated with an Aimcon ultrafilter (50 kDa cutoff) and the labeling efficiencies were measured by a ThermoFisher One Nanodrop.

2.5 Liposome Reconstitution of NavAb Channels

The POPE/POPG (3:1, w/w, Avanti Polar Lipids Inc.) lipids dissolved in chloroform were dried in clean glass tubes with argon gas first, and then in a vacuum desiccator for 4 hours to evaporate the residual organic solvent completely. The dried lipids were resuspended in reconstitution buffer containing 20 mM Hepes, 150 mM NaCl or 150 mM NMDG, pH7.5 (for smFRET imaging) or 20 mM Hepes, 150 mM KCl or CsCl, pH7.5 (for liposome flux assay). The liposomes were formed by sonication and then destabilized with 1% LMNG (Anatrace Inc). The purified NavAb protein was mixed with the lipid solution at a protein lipid ratio of 1:200 (w/w, for liposome flux assay) or 1:4,000 (w/w, for smFRET imaging), and the NavAb proteoliposomes were formed by detergent removal using Bio-beads SM2 (Bioad Inc).2.6 Liposome fluorescence flux assay.

The K^+ gradient between inside and outside of the liposomes is established by diluting the liposomes in the extraliposomal buffer 20 times containing 20 mM Hepes, 150 mM NMDG, pH7.5. The liposomes were incubated with 2 μM of ACMA fluorescence probes for ~5 min, then ACMA fluorescence was measured using a 96 well plate reader (FluoStar, Ex/Em = 390nm/460nm) for ~5 min. After valinomycin was added at a final concentration of 0.45 μM, the fluorescence measurements were resumed with the same optical settings for ~40 min. Proton-specific ionophore CCCP was used as the positive control, liposomes without K^+ gradient, or with K^+ gradients without valinomycin were used as negative controls. The NavAb channel activities were calculated from the normalized fluorescence readings using the equation:

$$A = (F_0 - F_{val})/F_{max}$$

Where F_0, F_{val} and F_{max} are the stead state ACMA fluorescence at initial, after adding valinomycin and the maximum quenching achieved by adding CCCP, respectively. The

relative activities of the NavAb channel were normalized against the WT proteoliposomes included in every batch of assays.

2.7 Single Molecule FRET Imaging

Flow chambers for smFRET imaging were prepared following the protocol of Joo et al (Joo 2012). An objective-based customized TIRF built on a Nikon TE-2000U inverted microscope (TE-2000s) with 100x APO TIRF NA1.49 objective lens, 532 nm and 640 nm lasers, was used for single molecule imaging (Fig. 2.6). Donor and acceptor emissions were separated by W-view Gemini beam splitter with chromatic aberration correction (Hamamatsu Inc.) carrying the 638 nm long-pass beam splitter, then cleaned by 585/65 nm and 700/75 nm bandwidth filters (Chroma Inc.). The images were collected by ImagEM X2 EMCCD camera (Hamamatsu Inc.). The proteoliposomes containing fluorophore-labeled NavAb channels were retained on the PEGlyated surface coated with biotinylated Anti-Histag antibodies (1:200 dilution, ThermoFisher Inc.). Fluorophores were excited by 532 nm laser (~10 W/cm2) and time-lapse movies were collected at 10 frames per second (i.e. time resolution of 100 ms). Typical recording times were ~3 min, with half bleaching times ~ 1min. All imaging buffers contained ~3 mM Trolox, 5 mM PCA and 15 μg/μL of PCD to enhance the photostability of the fluorophores. To achieve symmetrical ionic conditions, 50 uM β-escine was used to permeabilize liposomes. At least 3 batches of independent smFRET imaging were performed for each sample/condition. For every movie, there were ~500 molecules per field of view with ~100 molecules containing both acceptor and donor fluorophores. The smFRET traces were extracted and analyzed with the SPARTAN software and then manually picked following the criteria described in the previous studies (Roy 2008). The bin size of all histograms and contour maps was 0.03 and FRET contour plots were generated from the smFRET data of the first 5s.

For kinetic analysis, a four-state FRET model was used and the smFRET traces were idealized with the SPARTAN software first using the Baum-Welch, then the Maximum Point Likelihood algorithms.

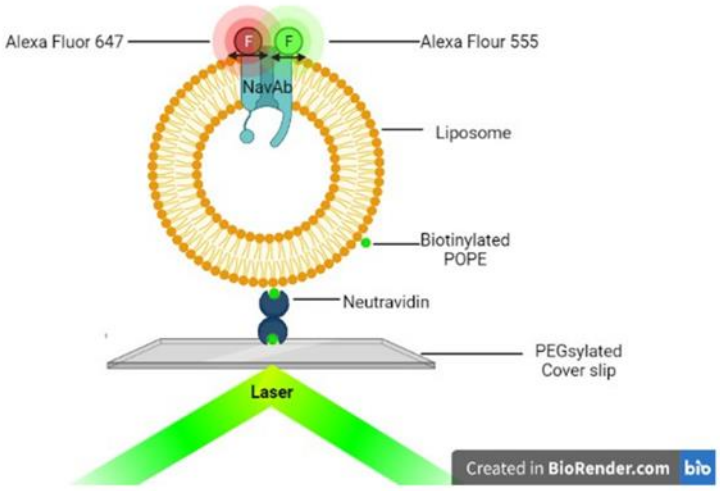

Figure 2.6 Experimental setup for smFRET imaging of a NavAb channel in liposome (created in BioRender.com)

CHAPTER 3

RESULTS

3.1 The NavAb Channel is Highly Conductive for Protons and Sodium Ions

The NavAb WT was reconstituted into liposomes (POPE:POPG = 3:1, w/w) with a protein lipid ratio of 1:200. In the presence of trans-liposomal K gradient (150 mM inside and 15 mM outside) and ionophore valinomycin, an electrical potential across liposomes was generated, which can be predicted by the Nernst equation. If the liposomes contain functional NavAb channel proteins with the cytoplasmic side facing the extra-liposomal side, the electrical potential will activate the NavAb channel and drive the proton and sodium ions into liposomes. As a result, the ACMA fluorophores will be protonated and trapped inside of the liposomes, leading to quenching of the ACMA fluorescence (Fig. 3.1a). My initial liposome fluorescence flux assay indicated that NavAb conducts protons, indicated by the drop of the ACMA fluorescence once the K ionophore valinomycin was added to establish the K Nernst potential (Fig. 3.1b, marked by arrow). As a positive control, in the presence of K Nernst potential, the proton uptake is more robust through the proton-specific ionophore CCCP. As a negative control, in the absence of the K gradient, the ACMA fluorescence does not change when the K ionophore valinomycin was added (Fig. 3.1b).

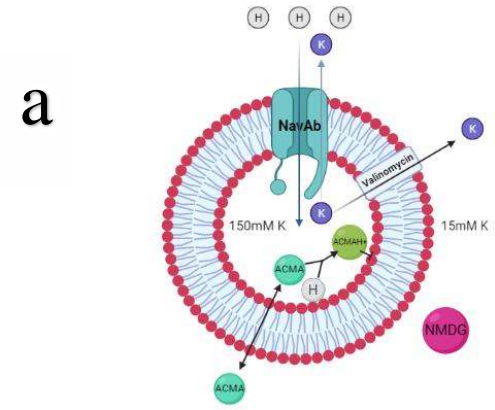

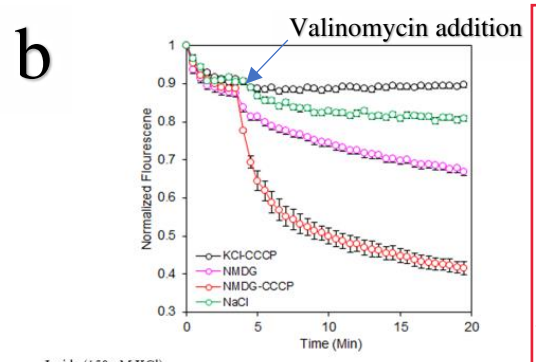

Inside (150mM KCl)
Outside (mM)

Name	KCl	NMDG	NaCl	CCCP
KCl-CCCP	150	-	-	1
NMDG	15	135	-	-
NMDG-CCCP	15	135	-	1
NaCl	15	-	135	-

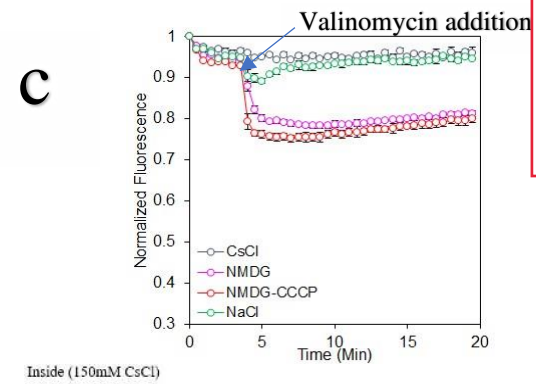

Inside (150mM CsCl)
Outside (mM)

Name	CsCl	NMDG	NaCl	CCCP
CsCl	150	-	-	-
NMDG	15	135	-	-
NMDG-CCCP	15	135	-	1
NaCl	15	-	135	-

I think the Nernst potential still exists but the only thing I worry about is the dynamic of having Na+ and H+ flowing in almost simultaneously pointing to a potential bottleneck effect. I kinda know this because even in our reference paper, they setup K inside and Na outside at same concs and that was not sufficient to open the channel until the addition of CCCP so we can almost think of it the same way with NavAb. Points more to NavAb xtics like conformational and other changes that might lead to quenching abolishment.

My future LFAs should entail the primary ion moving first triggering

Figure 3.1. Functional characterization of the NavAb proteins by liposome flux assay. (a) Cartoon illustration of the liposome fluorescence flux assay to determine channel activities of the NavAb channels (created with BioRender.com). (b) Proton and sodium uptake via the NavAb WT channel in liposomes, driven by K Nernst potential. Ionic conditions were listed in the table below. (c) Proton and sodium uptake via the NavAb WT channel in liposomes driven by Cs+ Nernst potential. Ionic conditions were listed in the table below. The data is presented as mean±ste, n=3.

When 150 mM NaCl was added to the outside of the liposomes, the ACMA fluorescence quenching was almost completely diminished, which indicates that the NavAb channel conducts sodium. As a result, the sodium influx mediated by the NavAb channel destroyed the K Nernst potential, therefore abolishing the proton uptake (Fig. 3.1b). We also noted that before adding the valinomycin, slower ACMA fluorescence quenching was observed when 150 mM KCl was included in the liposomes (Fig. 3.1b). Electrophysiological studies have shown that although the NavAb is relatively sodium selective, it has some low K conductivity as well. Thus, we hypothesized that the slow ACMA dropping prior addition of valinomycin was probably caused by the slow efflux of the K ions via the NavAb channel, which in turn drives the proton uptake through the NavAb channel. To test this hypothesis, we replace the intra-liposomal K+ ions with Cs^{+}, which are a non-permeant cation of the NavAb channel. Indeed, the slow drop of the ACMA fluorescence before adding valinomycin is almost abolished (Fig. 3.1c). We also noticed that the Cs+ gradient driven proton uptake through the NavAb channel is less robust than those driven by the K gradient, which probably is due to the relatively poor conductivity of the valinomycin to Cs+.

3.2 The NavAb WT Channel is Blocked by Lidocaine

Lidocaine is a classical blocker of the eukaryotic Navs, and electrophysiological studies showed that it can also block the prokaryotic NavAb channel. To explore the pharmacological profiles of the purified NavAb channel, we performed liposome fluorescence flux assays on the NavAb channels with different concentrations of lidocaine (Fig. 3.2a) My data showed that proton uptake via the NavAb channel is inhibited by lidocaine in a dose-dependent manner (Fig. 3.2b). The inhibition data was fitted with the Hill equation and predicted a half inhibition concentration of 2 mM, which is very close to that determined by patch-clamp studies on the NavAb channels expressed in cells (Gamal El-Din 2018).

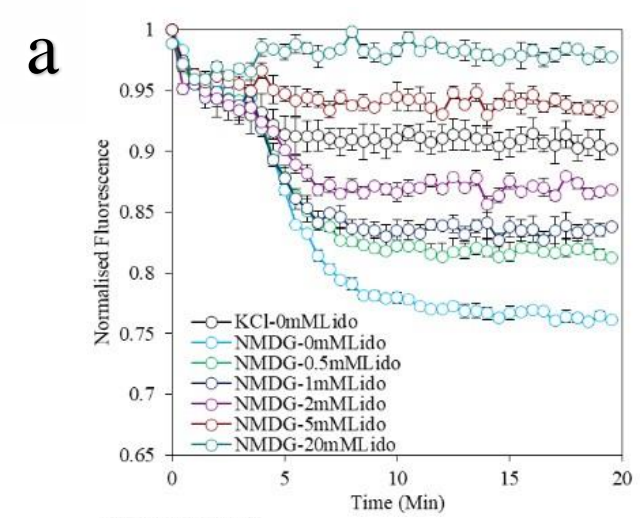

Inside (150mM KCl)
Outside (mM)

Name	KCl	NMDG	Lidocaine
KCl	150	-	-
NMDG-0mMLido	15	135	-
NMDG-0.5mMLido	15	135	.5
NMDG-1mMLido	15	135	1
NMDG-2mMLido	15	135	2
NMDG-5mMLido	15	135	5
NMDG-20mMLido	15	135	20

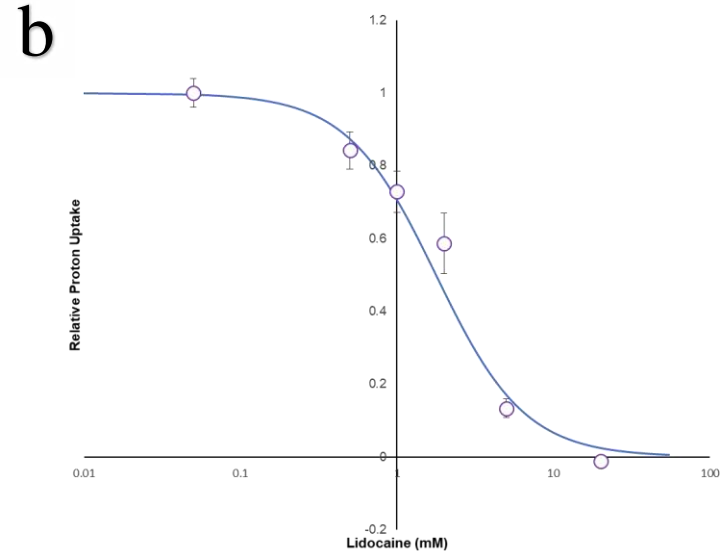

Figure 3.2. Lidocaine block of the NavAb channel. (a) Block of the proton uptake via the NavAb channel by lidocaine; (b) Dose-dependent inhibition of the proton uptake via the NavAb channel by lidocaine fitted by Hill equation. The data is presented as mean±ste, n=3.

3.3 The Tandem Dimeric and Tetrameric NavAb Channels are Functional

To implement smFRET studies on the NavAb channel, one major challenge is to label the tetrameric channel unit with a single FRET fluorophore pair. To achieve the goal, I have constructed the tandemeric NavAb channels, so that only 2 cysteine residues were introduced within 1 channel unit. Next, we constructed tandem dimeric NavAb channels with the channel unit assembled by 2 protomers and the tandem tetrameric NavAb channels with 1 channel unit containing only 1 protomer (Table 1). As described in the material and methods section, we obtained the tandem NavAb channels by expressing the tandem cDNAs with flexible linkers. For the tandem dimeric NavAb channel, introducing the cysteine residue at 1 subunit within the tandem dimeric protomer will generate channel molecules with 2 cysteine residues at diagonal subunits. To study the conformational dynamics of the NavAb channel selectivity filter, I introduced E189C, V190C mutations at the P1 helix of the selectivity filter (Fig. 3.31a), one at a time.

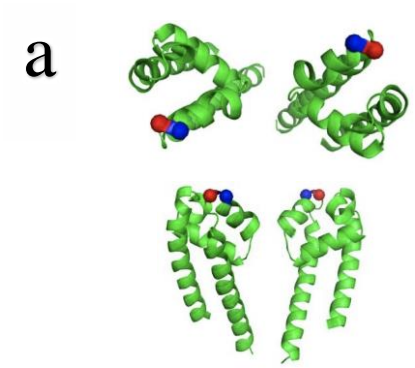

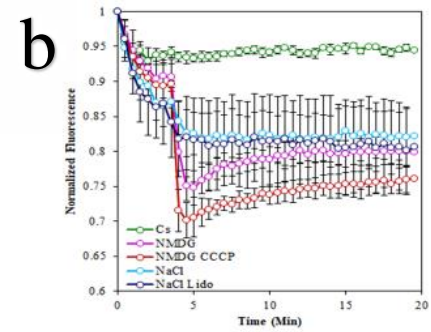

Inside (150mM CsCl)
Outside (mM)

Name	CsCl	NMDG	NaCl	CCCP
CsCl	150	-	-	-
NMDG	15	135	-	-
NMDG CCCP	15	135	-	1
NaCl	15	-	135	-
NaCl Lido	15	-	135	-

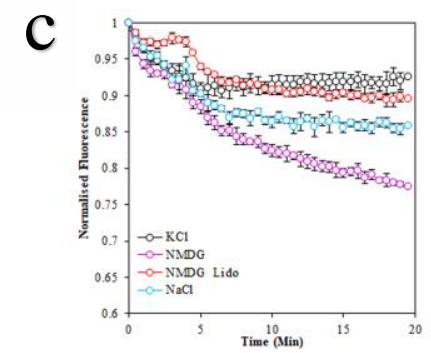

Inside (150mM KCl)
Outside (mM)

Name	KCl	NMDG	NaCl	Lidocaine
KCl	150	-	-	-
NMDG	15	135	-	-
NMDG Lido	15	135	-	5
NaCl	15	-	135	-

Figure 3.31. Liposome flux assay of the tandem dimeric NavAb[189C-WT] and NavAb2[190C-WT]. (a) Top and side view of the E189 and V190 residues in NavAb channel diagonal subunits. (b) Liposome flux assay of NavAb[189C-WT] with internal 150 CsCl. (c) Liposome flux assay of NavAb[190C-WT] with internal 150 KCl.

I then expressed and purified the tandem NavAb channels and reconstituted them into liposomes by following the same protocol for the NavAb WT described previously. Liposome fluorescence flux assays were performed on E189C-WT and V190C-WT mutants (Fig. 3.31a) and my data indicated that the two mutant proteins can conduct protons at a rate like that of the NavAb WT proteins and sensitive to lidocaine blocking (Fig. 3.31b,c). We also performed liposome fluorescence flux assay on the tandem tetramer NavAb channel (Fig. 3.32a). My results confirmed that subunit linkage does not interfere with the NavAb channel's ability to transport protons. Moreover, the pharmacology of the tandem tetrameric NavAb channel is also the same as the WT channel (Fig. 3.32b,c). Successful construction and production of the tandem NavAb channel allows us to label the NavAb channel with a single pair of FRET fluorophores and implement smFRET measurements on them.

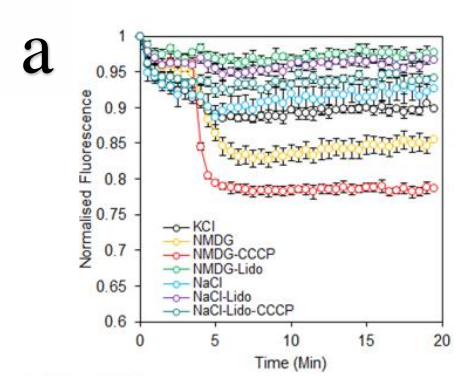

Inside (150mM KCl)
Outside (mM)

Name	KCl	NMDG	NaCl	Lidocaine	CCCP
KCl	150	-	-	-	-
NMDG	15	135	-	-	-
NMDG-CCCP	15	135	-	-	1
NMDG-Lido	15	135	-	5	-
NaCl	15	-	135	-	-
NaCl-Lido	15	-	135	5	-
NaCl-Lido-CCCP	15	-	135	-	1

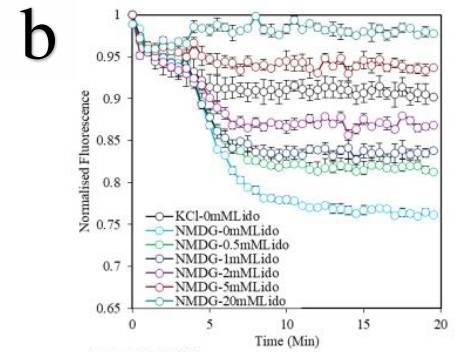

Inside (150mM KCl)
Outside (mM)

Name	KCl	NMDG	Lidocaine
KCl	150	-	-
NMDG-0mMLido	15	135	-
NMDG-0.5mMLido	15	135	.5
NMDG-1mMLido	15	135	1
NMDG-2mMLido	15	135	2
NMDG-5mMLido	15	135	5
NMDG-20mMLido	15	135	20

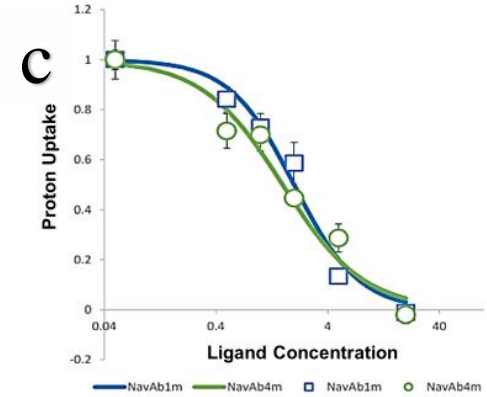

Figure 3.32. Functional characterization of the tandem tetrameric NavAb channels. All ionic and pharmacologic conditions seen in table under figures (a) Liposome flux assay of the tandem tetrameric NavAb channel. (b) Lidocaine blockade of the the tandem tetrameric NavAb channel. (c) Dose dependent inhibition of the monomeric (NavAb1m) and tandem tetrameric (NavAb4m) NavAb channel by lidocaine, fitted with Hill equation.

3.4 Structural Dynamics of the NavAb Selectivity Filter Revealed by smFRET

To examine the real time conformational dynamics of the NavAb selectivity filter, two NavAb constructs were made to express the tandem dimeric NavAb channel with 2 cysteine residues locating at E189C of the diagonal subunits (named as NavAb2mE189C), and the tandem tetrameric NavAb channel with 2 cysteine residues locating at E189C of the adjacent subunits (named as NavAb4m(189C)2-(WT)2). We purified the two NavAb tandem proteins and then labeled them with the Alexa fluor 555 and 647 c2 maleimide FRET pair. The fluorophore labeled proteins were reconstituted into liposomes (POPE:POPG = 3:1 w/w) with a protein lipid ratio of 1:4000 (w/w), so that the liposome populations are dominant by these either empty or containing only 1 NavAb channel molecule. The NavAb liposomes were immobilized to the PEGlyated coverslip surface using an anti-HisTag antibody so that only the NavAb proteoliposomes with N-terminal HisTag at the outside can be retained on the surface. Since the smFRET data from the NavAb proteoliposomes containing multiple channel molecules will be excluded for their multiple bleaching steps in donor and acceptor fluorophores, the sample immobilization using anti-HisTag antibody allows us to control the NavAb channel orientations, which are important for applying and switch voltages. Using a trans-liposomal K+ or Na+ gradient (150 mM outside and ~0.05 mM inside, corresponding to 0.05 mM at cytosolic side and 150 mM at the extracellular side) and ionophore valinomycin(K+)/monensin(Na+), an electric potential of -200mv can be generated and applied on the NavAb channel in liposomes.

As I have described previously, the selectivity filter of sodium channels is structurally and functionally distinct from those of K channels. Voltage-gated sodium channels permeate partially hydrated Na+ while K channels permeate fully dehydrated K+. Previous smFRET

studies on the selectivity filter of a K channel showed that ions have significant impacts on the conformation dynamics of the selectivity filter (Wang 2019). Specifically, K+ ions induce compact and rigid conformations with very minimized changes, while in the presence of Na+, the K selectivity filter exhibits dilated conformation with high and frequent dynamics. The smFRET data indicated that dehydrated K+ in the selectivity pore coordinates with four subunits simultaneously, acting as a bridge to constrict or stabilize the conformations of the selectivity filter pore. However, the size and ionic hydration shells of the Na+ do not endorse the same coordination of Na+ with the K selectivity filter pore, therefore, leading to the dilated and dynamic conformations. Since the structure and ion binding site of the selectivity filter pore in NavAb is very different from those of K channels, it would be interesting to explore whether the K+ and Na+ have differential effects on its conformation.

As described in the material and method section, I performed smFRET imaging on the NavAb channel mutants with FRET fluorophore pair labeling at the E189C residues locating at either diagonal or adjacent subunits. As shown by Fig. 3.41a, the donor or acceptor fluorophores are all bleached in one step, which indicates that these NavAb molecules imaged carry a single fluorophore pair. Moreover, their fluorescence intensities are strongly anti-correlated, indicating that the FRET changes reflect the conformational changes at the selectivity filter, rather than the photophysics of the fluorophores. The three traces shown in Fig. 3.41a,b,c were obtained from the NavAb channel with FRET fluorophore pair labeling at the E189C of the adjacent subunits, but similar traces were also seen in the NavAb channel with FRET fluorophore pair labeling at the E189C of the diagonal subunits (data not shown). Significant numbers of FRET traces exhibit spontaneous FRET changes under all ionic and voltage conditions (Fig. 3.41a,b,c). The smFRET traces from both NavAb mutants are very

heterogenous with 30~50% of traces being dynamic, while other traces exhibiting constant FRET without significant changes.

As described previously, once activated by depolarization voltage, the NavAb channel enters an inactivation state in less than 100 ms, which probably is caused by the collapse of the selectivity filter. The inactivation can only be removed when the NavAb channel is deactivated. In other words, the conformations of the selectivity filter are dependent on voltage, which is at conductive state under resting voltage, at non or low conductive state upon activating voltage. First, we examined the effects of K+, Na+ and blocker lidocaine on the NavAb selectivity filter by smFRET. Histograms from over hundreds of individual NavAb molecules, under resting voltage, with fluorophore pair labeling at E189C of either diagonal or adjacent subunits showed 3 major FRET populations, with peaks at 0.2, 0.4 and 0.8, respectively. Unlike the selectivity filter of the K channels, only very minimized ion dependent FRET changes were observed on the NavAb selectivity filter (Fig. 3.42 b, c). The most significant changes in FRET distributions were caused by 5 mM Lidocaine, which binds at the inner cavity while projecting into the selectivity filter (Fig. 3.42b,c). My smFRET indicated that interactions between the ions and selectivity pore are weak in the NavAb channel, probably because it conducts partially dehydrated Na^+ and K^+. If the smFRET faithfully reports the conformational dynamics of the NavAb selectivity filter, charge and size may not be the primary mechanism underlying its ion selectivity. In addition, my smFRET data also showed that lidocaine may block the NavAb channel by altering the conformations of the selectivity filter.

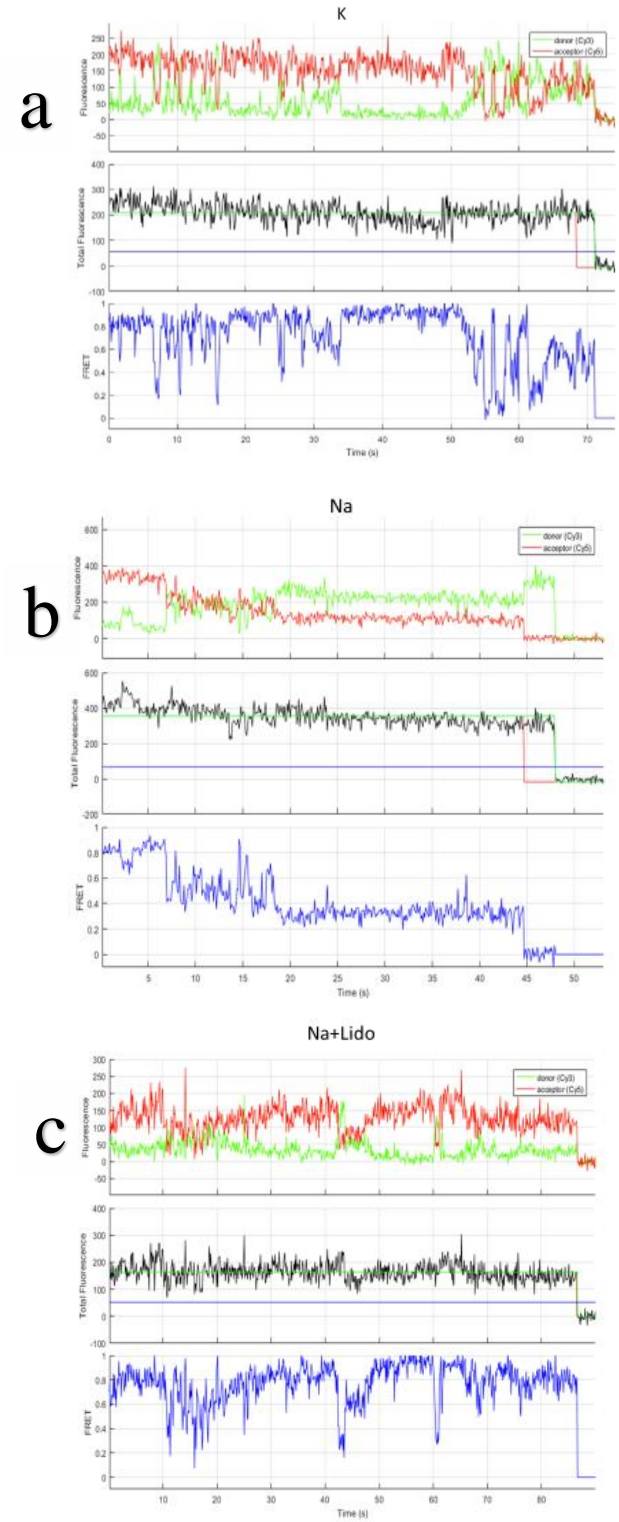

Figure 3.41 Representative smFRET traces from the tandem tetrameric NavAb channel. Donor and acceptor fluorophore labeling at E189C the adjacent subunits, in the presence of (a) 150mM KCl (b) 150mM NaCl (c) 150mM NaCl and 5mM Lidocaine at the cytoplasmic side.

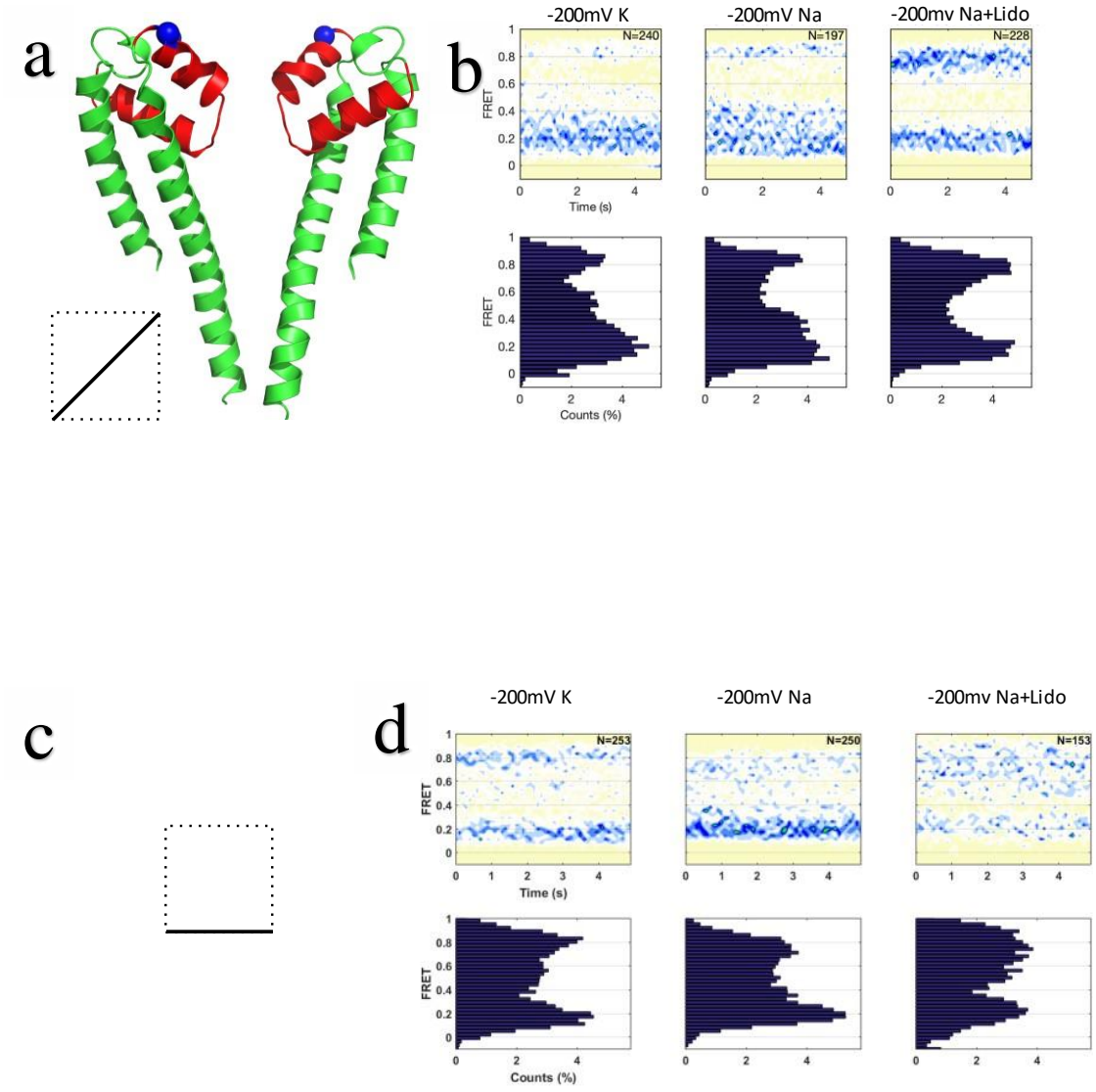

Figure 3.42. Histograms and contour maps of the smFRET data from the NavAb channel. Donor and acceptor fluorophore labeling at the E189C of diagonal (b) or adjacent (c, d) subunits. The E189 residues at the diagonal subunits were highlighted as red spheres (a). Bin size is 0.03.

3.5 Structural Basis of Slow Inactivation

The conductance of the NavAb channel decreases in less than 100 ms after the channel is activated, a phenomenon known as slow inactivation. Slow inactivation is important for regulating the excitability of neurons and many other cells. Both Navs and Cavs are capable of slow inactivation, but eukaryotic orthologs have a different inactivation mechanism, known as fast inactivation. The fast inactivation has distinct mechanisms, which occurs due to the voltage dependent protrusion of the flexible linker into the ion conduction pathway. To assess the role of the selectivity filter in slow inactivation, smFRET measurements were performed on the E189C labeling sites at the diagonal or adjacent subunit, under -200mV and 0mV in the presence of Na^+, K^+ and lidocaine. In the presence of K^+, no significant changes in FRET distributions were observed between -200mV and 0mV groups (Fig. 3.5a,d). However, in the presence of Na+, very subtle differences between the resting 200 mV and activating 0 mV appeared, they are not consistent between the two different labeling configurations, i.e diagonal and adjacent subunits (Fig. 3.5b,e). The lidocaine group was also quite similar between the voltage conditions, but a FRET population with peak at 0.4 appears (Fig. 3.5c,f). It should be noted that all these results are preliminary and smFRET histograms and contour maps were generated from slightly over 100 molecules. More data collection would potentially increase the smoothness of the data, as well as the confidence in the conclusions. Overall, my preliminary smFRET data displayed surprisingly very changes in structural dynamics of the NavAb selectivity filter under all conditions.

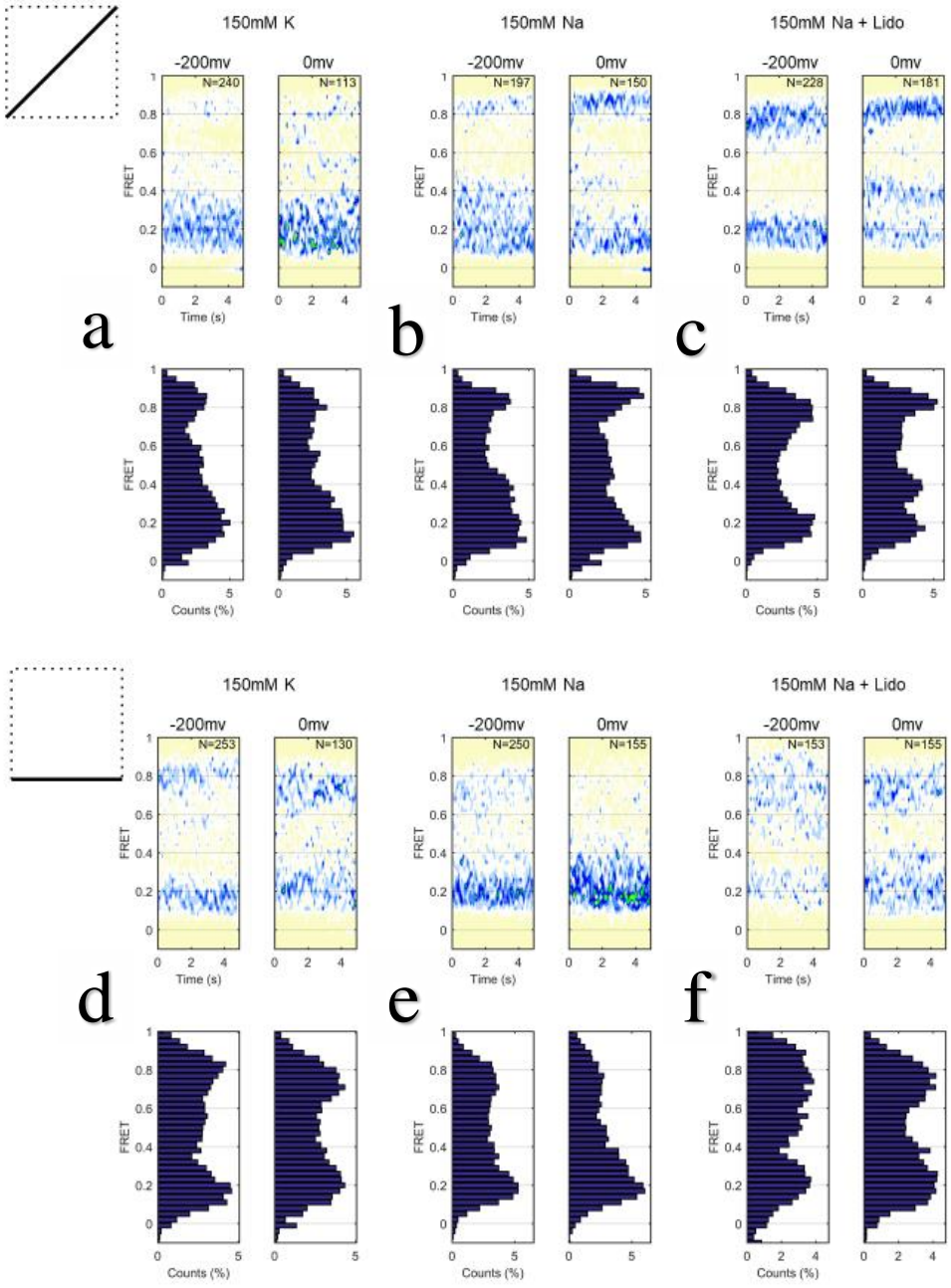

Figure 3.5 Structural Basis of Slow Inactivation. Histograms and contour maps of the smFRET data from E189C at diagonal (a, b, c) and adjacent (d, e, f) subunits, in the presence of 150mM KCl (a, d), 150mM NaCl (b, e), and 150mM NaCl and 5mM Lidocaine (c, f). Bin size is 0.03.

CHAPTER 4

DISCUSSION

Voltage-gated ion channels are associated with many neuronal, muscular, and cardiovascular diseases and are important drug targets. Exploration of the dynamic nature of VGSC's in lipid environments is essential to better understandings on some fundamental mechanistic questions. In the present project, I studied the function and structure of a prokaryotic NavAb channel to (a) functionally characterize its validity as a model voltage-gated sodium channel, (b) the overall structural dynamics of the Na selectivity filter and their implications to ion selectivity, (c) the potential mechanisms of the lidocaine blockade of the NavAb. The selectivity filter is key to its ion selectivity and close to targeting sites of many VGSC blocking drugs. Although ion selectivity in voltage-gated sodium channels based on size and charge have been extensively studied by electrophysiological and structural approaches, the structural flexibility of the selectivity filter under ambient temperatures, in native lipid environment and within functional channels has never been experimentally examined.

In the present work, I constructed and purified the NavAb proteins and reconstituted them into liposomes that mimicked their native membrane environments. Using a robust liposomal flux assay, we established that the NavAb channel is highly permeable to Na^+ and H^+, low permeable to K^+, not permeable to Cs^+ and bulky organic cation NMDG. I also showed that lidocaine, a classical voltage-gated sodium channel blocker in wide clinic use, blocks the NavAb channel with an affinity close to these determined by electrophysiological studies on

eukaryotic Navs. These results are also consistent with the previous patch-clamp studies on the NavAb channels expressed in insect cells (Payandeh 2011).

To study the conformational dynamics of the NavAb selectivity filter, I created the constructs which allow us to examine the FRET changes on the labeling sites at diagonal and adjacent subunits, so the smFRET data from the two labeling configurations can be cross validated. I established again through liposome flux assay that both the tandem dimeric and tetrameric mutant channels are functional to conduct H^+ and their pharmacological profiles, in terms of the lidocaine, are like that of WT channels.

I set out to investigate the dynamics of the selectivity filter by smFRET under different ionic conditions to elucidate the potential ion channel interactions within the selectivity filter pore, in the presence of lidocaine to test its potential impacts on the selectivity filter dynamics, and under activating (0 mV) and resting (-200 mV) voltages to uncover the structural basis underlying slow inactivation. Surprisingly, the NavAb selectivity filter has very subtle ion-dependent conformational changes, which implies much weaker interactions than those observed on the K channel selectivity filter. The coordination between K+ and the K selectivity filters is symmetric and matches the channel symmetry well. However, the partially hydrated Na+ is highly asymmetric, therefore the selectivity filter pore in NavAb should also be asymmetric to facilitate the ion channel interactions. Therefore, the spontaneous FRET changes perhaps reflect the real time symmetry changes in the NavAb channel. As I have discussed previously in the results section, the large, spontaneous FRET changes indicate that the size of the selectivity filter pore varies in a scale that may invalidate the current view that ion selection is based on size. Therefore, other mechanisms may play a determinant role in the origins of the NavAb ion selectivity. The symmetry of the channel structures and ions could

potentially be a high-profile mechanism to be investigated. In addition, since calcium selective mutant CavAb differs from NavAb by on three residues within the selectivity filter pore, comparison of the dynamics of both NavAb and CavAb channels under different ionic conditions may grant novel mechanistic insights into ion selectivity.

Since lidocaine binds to the inner cavity of NavAb immediately underneath the selectivity filter, we hypothesized that lidocaine may also exert its inhibitory effects by modifying the selectivity filter dynamics. Previous models had suggested that lidocaine inhibits NavAb by destabilizing the closed state. My smFRET showed that lidocaine dramatically stabilizes the high FRET populations of the NavAb selectivity. The structural effects of lidocaine were observed from both labeling configurations, i.e the E189C sites at the diagonal and adjacent subunits. This effect may be reasonable, for lidocaine binding at the inner cavity may serve as a bridge by interacting with the residues of all 4 NavAb subunits, including those on the selectivity filter. As a result, the stability of the entire tetrameric channel unit, as well as the selectivity filter pore are significantly increased. To further investigate this phenomenon, it would be very helpful to examine selectivity filter dynamics under a range of lidocaine concentrations. If the enrichments of the high FRET population of NavAb selectivity filter exhibit a dose dependent manner, with a similar affinity as that determined by liposome flux assay or previous patch-clamp physiology, it will not only confirm its effect, but uncover a potential structural mechanism underlying lidocaine blockade. It would also be interesting to see if larger NavAb blocking drugs like flecainide would have similar effects on selectivity filter dynamics.

Slow inactivation from selectivity filter collapse is thought to occur after NavAb channel activation. We observed very subtle differences under both the resting and activating

voltages. My results could either question whether selectivity filter collapse is the underlying mechanism of slow inactivation or suggest that the conformational changes at the selectivity filter that causes slow inactivation are too small to be detected by smFRET.

In summary, my liposome fluorescence flux assays clearly indicate the NavAb channel is a genuine voltage-gated sodium channel that can serve as a valid model channel to probe the structure and function relationship of the Navs. My smFRET data indicated that ion selectivity based on size and charge need to be further investigated, based on the significant conformational dynamics reported. In this sense, ion selectivity based on symmetry could be a novel mechanism that remains to be validated. My research uncovered the structural dynamics of the NavAb selectivity filter and provided novel insights into the mechanisms underlying ion selectivity in VGSCs.

REFERENCE LIST

Arcisio-Miranda, Manoel, Yukiko Muroi, Sandipan Chowdhury, and Baron Chanda. 2010. "Molecular Mechanism of Allosteric Modification of Voltage-Dependent Sodium Channels by Local Anesthetics." *The Journal of General Physiology* 136, no. 5: 541–54. https://doi.org/10.1085/jgp.201010438.

Beneski, D A, and W A Catterall. 1980. "Covalent Labeling of Protein Components of the Sodium Channel with a Photoactivable Derivative of Scorpion Toxin." *Proceedings of the National Academy of Sciences of the United States of America* 77, no. 1: 639–43. https://doi.org/10.1073/pnas.77.1.639.

Callahan, Karen M, and Benoît Roux. 2018. "Molecular Dynamics of Ion Conduction through the Selectivity Filter of the Na(V)Ab Sodium Channel." *The Journal of Physical Chemistry. B* 122, no. 44: 10126–42. https://doi.org/10.1021/acs.jpcb.8b09678.

Catterall, William A. 2014. "Structure and Function of Voltage-Gated Sodium Channels at Atomic Resolution." *Experimental Physiology* 99, no. 1: 35–51. https://doi.org/10.1113/expphysiol.2013.071969.

Catterall, William A. 2017. "Forty Years of Sodium Channels: Structure, Function, Pharmacology, and Epilepsy." *Neurochemical Research* 42, no. 9: 2495–2504. https://doi.org/10.1007/s11064-017-2314-9.

Catterall, William A., Michael J. Lenaeus, and Tamer M. Gamal El-Din. 2020. "Structure and Pharmacology of Voltage-Gated Sodium and Calcium Channels." *Annual Review of Pharmacology and Toxicology* 60, no. 1: 133–54. https://doi.org/10.1146/annurev-pharmtox-010818-021757.

Catterall, William A, and Teresa M Swanson. 2015. "Structural Basis for Pharmacology of Voltage-Gated Sodium and Calcium Channels." *Molecular Pharmacology* 88, no. 1: 141–50. https://doi.org/10.1124/mol.114.097659.

Catterall, William A, Goragot Wisedchaisri, and Ning Zheng. 2020. "The Conformational Cycle of a Prototypical Voltage-Gated Sodium Channel." *Nature Chemical Biology* 16, no. 12: 1314–20. https://doi.org/10.1038/s41589-020-0644-4.

Chakrabarti, Nilmadhab, Christopher Ing, Jian Payandeh, Ning Zheng, William A Catterall, and Régis Pomès. 2013. "Catalysis of Na+ Permeation in the Bacterial Sodium Channel Na(V)Ab." *Proceedings of the National Academy of Sciences of the United States of America* 110, no. 28: 11331–36. https://doi.org/10.1073/pnas.1309452110.

Finol-Urdaneta, Rocio K, Yibo Wang, Ahmed Al-Sabi, Chunfeng Zhao, Sergei Y Noskov, and Robert J French. 2014. "Sodium Channel Selectivity and Conduction:

Prokaryotes Have Devised Their Own Molecular Strategy." *The Journal of General Physiology* 143, no. 2: 157–71. https://doi.org/10.1085/jgp.201311037.

Gamal El-Din, Tamer M, Michael J Lenaeus, Ning Zheng, and William A Catterall. 2018. "Fenestrations Control Resting-State Block of a Voltage-Gated Sodium Channel." *Proceedings of the National Academy of Sciences of the United States of America* 115, no. 51: 13111–16. https://doi.org/10.1073/pnas.1814928115.

Heinemann, Stefan H., Heinrich Terlau, Walter Stühmer, Keiji Imoto, and Shosaku Numa. 1992. "Calcium Channel Characteristics Conferred on the Sodium Channel by Single Mutations." *Nature* 356, no. 6368: 441–43. https://doi.org/10.1038/356441a0.

Hille, B. 1975. "Ionic Selectivity, Saturation, and Block in Sodium Channels. A Four-Barrier Model." *The Journal of General Physiology* 66, no. 5: 535–60. https://doi.org/10.1085/jgp.66.5.535.

Hille, B. 1978. "Ionic Channels in Excitable Membranes. Current Problems and Biophysical Approaches." *Biophysical Journal* 22, no. 2: 283–94. https://doi.org/10.1016/S0006-3495(78)85489-7.

Hodgkin, A L, and A F Huxley. 1952. "A Quantitative Description of Membrane Current and Its Application to Conduction and Excitation in Nerve." *The Journal of Physiology* 117, no. 4: 500–544. https://doi.org/10.1113/jphysiol.1952.sp004764.

Hondeghem, L M, and B G Katzung. 1984. "Antiarrhythmic Agents: The Modulated Receptor Mechanism of Action of Sodium and Calcium Channel-Blocking Drugs." *Annual Review of Pharmacology and Toxicology* 24, no. 1: 387–423. https://doi.org/10.1146/annurev.pa.24.040184.002131.

Irie, Katsumasa, Yukari Haga, Takushi Shimomura, and Yoshinori Fujiyoshi. 2018. "Optimized Expression and Purification of NavAb Provide the Structural Insight into the Voltage Dependence." *FEBS Letters* 592, no. 2: 274–83. https://doi.org/10.1002/1873-3468.12955.

Joo, Ha T. 2012."Labeling proteins for single-molecule FRET". Cold Spring Harb Protoc. doi: 10.1101/pdb.prot071035.

Kühlbrandt, Werner. 2016. "Three in a Row-How Sodium Ions Cross the Channel." *The EMBO Journal* 35, no. 8: 793–95. https://doi.org/10.15252/embj.201694094.

Lenaeus, Michael J., Tamer M. Gamal El-Din, Christopher Ing, Karthik Ramanadane, Régis Pomès, Ning Zheng, and William A. Catterall. 2017. "Structures of Closed and Open States of a Voltage-Gated Sodium Channel." *Proceedings of the National Academy of Sciences* 114, no. 15: E3051. https://doi.org/10.1073/pnas.1700761114.

Lerner, Eitan, Anders Barth, Jelle Hendrix, Benjamin Ambrose, Victoria Birkedal, Scott C Blanchard, Richard Börner, et al. 2021. "FRET-Based Dynamic Structural Biology:

Challenges, Perspectives and an Appeal for Open-Science Practices." Edited by Olga Boudker. *ELife* 10, no. March: e60416. https://doi.org/10.7554/eLife.60416.

Nau, Carla, Sho-Ya Wang, and Ging Kuo Wang. 2003. "Point Mutations at L1280 in $Na_v1.4$ Channel D3-S6 Modulate Binding Affinity and Stereoselectivity of Bupivacaine Enantiomers." *Molecular Pharmacology* 63, no. 6: 1398. https://doi.org/10.1124/mol.63.6.1398.

Naylor, Claire E, Claire Bagnéris, Paul G DeCaen, Altin Sula, Antonella Scaglione, David E Clapham, and B A Wallace. 2016. "Molecular Basis of Ion Permeability in a Voltage-Gated Sodium Channel." *The EMBO Journal* 35, no. 8: 820–30. https://doi.org/10.15252/embj.201593285.

Ngo, Van, Yibo Wang, Stephan Haas, Sergei Y Noskov, and Robert A Farley. 2016. "K+ Block Is the Mechanism of Functional Asymmetry in Bacterial Na(v) Channels." *PLoS Computational Biology* 12, no. 1: e1004482–e1004482. https://doi.org/10.1371/journal.pcbi.1004482.

Payandeh, Jian, Todd Scheuer, Ning Zheng, and William A Catterall. 2011. "The Crystal Structure of a Voltage-Gated Sodium Channel." *Nature* 475, no. 7356: 353–58. https://doi.org/10.1038/nature10238.

Roy, Rahul, Sungchul Hohng, and Taekjip Ha. 2008. "A Practical Guide to Single-Molecule FRET." *Nature Methods* 5, no. 6: 507–16. https://doi.org/10.1038/nmeth.1208.

Stephens, Robert F., W. Guan, Boris S. Zhorov, and J. David Spafford. 2015. "Selectivity Filters and Cysteine-Rich Extracellular Loops in Voltage-Gated Sodium, Calcium, and NALCN Channels." *Frontiers in Physiology* 6: 153. https://doi.org/10.3389/fphys.2015.00153.

Tang, Lin, Tamer M Gamal El-Din, Jian Payandeh, Gilbert Q Martinez, Teresa M Heard, Todd Scheuer, Ning Zheng, and William A Catterall. 2014. "Structural Basis for Ca2+ Selectivity of a Voltage-Gated Calcium Channel." *Nature* 505, no. 7481: 56–61. https://doi.org/10.1038/nature12775.

Tang, Lin, Tamer M Gamal El-Din, Teresa M Swanson, David C Pryde, Todd Scheuer, Ning Zheng, and William A Catterall. 2016. "Structural Basis for Inhibition of a Voltage-Gated Ca(2+) Channel by Ca(2+) Antagonist Drugs." *Nature* 537, no. 7618: 117–21. https://doi.org/10.1038/nature19102.

Wang, Shizhen, Sun-Joo Lee, Grigory Maksaev, Xin Fang, Chong Zuo, and Colin G Nichols. 2019. "Potassium Channel Selectivity Filter Dynamics Revealed by Single-Molecule FRET." *Nature Chemical Biology* 15, no. 4: 377–83. https://doi.org/10.1038/s41589-019-0240-7.

Wang, Shizhen, Reza Vafabakhsh, William F Borschel, Taekjip Ha, and Colin G Nichols. 2016. “Structural Dynamics of Potassium-Channel Gating Revealed by Single-Molecule FRET.” *Nature Structural & Molecular Biology* 23, no. 1: 31–36. https://doi.org/10.1038/nsmb.3138.

Wisedchaisri, Goragot, Lige Tonggu, Eedann McCord, Tamer M Gamal El-Din, Liguo Wang, Ning Zheng, and William A Catterall. 2019. “Resting-State Structure and Gating Mechanism of a Voltage-Gated Sodium Channel.” *Cell* 178, no. 4: 993-1003.e12. https://doi.org/10.1016/j.cell.2019.06.031.

Yue, Lixia, Betsy Navarro, Dejian Ren, Arnolt Ramos, and David E Clapham. 2002. “The Cation Selectivity Filter of the Bacterial Sodium Channel, NaChBac.” *The Journal of General Physiology* 120, no. 6: 845–53. https://doi.org/10.1085/jgp.20028699.

VITA

Joshua Lee Vance was born November 19, 1994, in Blue Springs, Missouri. He was educated in a mix of public and private schools and graduated from Bolivar High School in 2013. He received an Excellence Scholarship to the University of Missouri, Columbia, in Columbia Missouri. His degree was Bachelor of Science in Biology. After working a year as a Forensic Scientist at Quest Diagnostics in Lenexa Kansas and being awarded for speed and accuracy in lab, he began a Cell and Molecular Biology Master's program at University of Missouri, Kansas City. Upon completion of Degree requirements, he plans to work in the pharmaceutical research industry.